ARTICLE IN PRESS

Computers and Mathematics with Applications xxx (xxxx) xxx

Contents lists available at ScienceDirect

Computers and Mathematics with Applications

journal homepage: www.elsevier.com/locate/camwa

On the mathematical modeling of inflammatory edema formation

Ruy Freitas Reis [b,*], Rodrigo Weber dos Santos [a,b], Bernardo Martins Rocha [a,b], Marcelo Lobosco [a,b]

[a] Graduate Program on Computational Modeling, Federal University of Juiz de Fora, Minas Gerais, Brazil
[b] Computer Science Department, Federal University of Juiz de Fora, Minas Gerais, Brazil

ARTICLE INFO

Article history:
Available online xxxx

Keywords:
Computational immunology
Edema modeling
Porous media
Partial differential equations
Biot

ABSTRACT

When pathogens enter into the body, the natural defense reaction is an immunological process triggered by the production of cytokines by macrophages. This reaction is called inflammation and it is an important and complex physiological response of living tissues to all harmful damages. As a consequence of the immune response, the most common symptoms are edema, redness, fever, and pain. All of these four symptoms are related to the physiological process of the immune defense system. For instance, edema may be caused by increased blood vessel wall permeability which leads to a swell at the infection site. So, edema is a consequence of interstitial fluid dynamics and its interactions with the immune system. In this present study, this physiological process is mathematically described by a nonlinear system of partial differential equations (PDE) based on a porous media approach. The model describes the interaction between the neutrophils and the pathogen, which in our case is non-specific bacteria. In addition, a poroelastic model is coupled with the inflammatory one resulting in an hydro-mechanical model for inflammatory edema. The new suggested model was able to reproduce key aspects of an inflammatory edema formation.

1. Introduction

Edema is often one of four classical symptoms of an inflammatory reaction followed by redness, fever, and pain [1]. These symptomatic behaviors are consequences of the physiologic process in a living body. The body temperature increases as a consequence of an elevation in the concentration of proinflammatory cytokines [2], the redness is a reflex of vasodilation. The pain is a result of chemical irritation of nerve endings in addition to mechanical compression, and finally, the swelling is a result of the increase in vascular permeability [3].

When a living body becomes infected by a pathogen, an inflammatory reaction is triggered by the immune system as an attempt to control and protect the infection site against invading organisms [4,5]. Some mediators of the inflammatory response, like histamine and kinins, induce vasodilation. The increase of vascular permeability allows immune cells to go to the infection site [1]. The immune cells extravasation also increases the blood plasma flux into the infected area. Fluid accumulation contributes to tissue swelling, forming an edema [1]. In addition, this fluid accumulation may increase the plasma volume up to 5 or 7 times [3].

* Correspondence to: Rua José Lourenço Kelmer, s/n - Martelos, Juiz de Fora, MG, Brazil.
E-mail address: ruyfreitas@ice.ufjf.br (R.F. Reis).

https://doi.org/10.1016/j.camwa.2019.03.058
0898-1221/

Edema may occur in different places of the body, such as the heart, lungs, legs, arms, and others [6–9]. Edema is also classified as intracellular or extracellular, depending upon the local where the accumulation of excess fluid occurs, inside or outside the cell, respectively. The present study considers just extracellular edema which can be caused by an increase of capillary pressure, reduction of plasma proteins, lymphatic system dynamics, and an increase of capillary permeability [3].

The fluid accumulation may lead to health problems such as in the heart muscle, *e.g.* only 3.5% of increase in myocardial water content leads to a reduction of the cardiac output by 40% [7]. So, models to simulate the dynamics of fluid accumulation in the body may be helpful to better understand some challenging health problems.

Mathematical models that describe the interactions between pathogens and the human immune system (HIS) are not new and can be found in several previous work [10–12]. The mathematical model used in this study to simulate the HIS is based on previous work [13]. This HIS model was then extended to include some key aspects of the edema formation [14,15]. Moreover, there are some studies that model interstitial fluid pressure (IFP) dynamics [16–18]. An initial model that combines IFP dynamics and the immune system regarding the key aspects of an edema formation was first suggested in our previous work [15].

The classical theory of poroelasticity mechanics of a fluid-saturated porous media was first proposed in 1941 [19], and since then it is widely used in several studies [20–22], and its application to living tissue is not new and still being used in present-day studies [23–25].

To the best of our knowledge, there are no previous studies on the coupling of the immune system with poroelasticity theory and its application to modeling an inflammatory edema formation. So, the key contribution of the present paper is a coupled model of the immune system with poroelasticity mechanics theory applied to a living tissue including the feedback of the mechanical deformation to the immune system model. It is worthwhile to highlight that in previous work [14,15] the fluid accumulation was not considered, but it occurs in edema. So, the present study comes up with a closure strategy to consider poroelasticity mechanics theory for modeling inflammatory edema and fluid accumulation, once we are considering a deformable porous medium. Although the model is presented in its general three-dimensional form, it is numerically solved in a one-dimensional domain, to ease the interpretation of the results of the coupled model. The numerical solution of the resulting PDE system solution is obtained using finite volume method (FVM) in a one-dimensional domain, and the stability of the numerical method is ensured using a first order upwind (FOU) scheme [26,27].

2. Methods

In this section, we present the mathematical model and the numerical methods used to obtain the simulation results.

2.1. Mathematical model

In this section, we present the detailed mathematical model used to perform our simulations. However, before presenting the equations, it is worthwhile to notice that the mathematical model is under the assumption of a porous media approach. Thus, we consider ϕ_s and ϕ_f as solid and fluid fractions, respectively, where fluid represents the interstitial fluid and solid the extracellular matrix along with the tissue cells, *i.e.*

$$\phi_f = \frac{V_f}{V} = 1 - \frac{V_s}{V} = 1 - \phi_s, \tag{1}$$

where V_f, V_s and V are the fluid volume, solid volume and total volume, respectively.

2.1.1. Neutrophil–bacteria inflammatory model

The interaction between bacteria and neutrophil is modeled by a system of partial differential equations (PDE's) [14]. Non-specific bacteria are modeled by:

$$\begin{cases} \dfrac{\partial(\phi_f C_b)}{\partial t} = \nabla \cdot (D_b \phi_f \nabla C_b) - r_b + q_b & \text{in } \Omega \times I, \\ D_b \phi_f \nabla C_b \cdot \vec{n} = 0 & \text{in } \partial\Omega \times I, \\ C_b(\cdot, 0) = C_{b0} & \text{in } \Omega, \end{cases} \tag{2}$$

where $\Omega \subset \mathbb{R}^n$ and $I = (0, t_f] \subset \mathbb{R}^+$ is the time interval, $C_b : \Omega \times I \to \mathbb{R}^+$ is the bacteria concentration on the interstitial fluid, ϕ_f is the porosity, D_b is the diffusion coefficient of the bacteria on interstitial fluid, q_b denotes the bacteria reproduction, and r_b denotes the bacterial death due to neutrophils action.

The following equation represents the bacterial source:

$$q_b = c_b \phi_f C_b, \tag{3}$$

where c_b is the growth rate into the interstitial tissue.

Please cite this article as: R.F. Reis, R.W. dos Santos, B.M. Rocha et al., On the mathematical modeling of inflammatory edema formation, Computers and Mathematics with Applications (2019), https://doi.org/10.1016/j.camwa.2019.03.058.

The function r_b denotes the action of neutrophils over bacteria leading to death. Represented by the following function:

$$r_b = \lambda_{nb}\phi_f C_n C_b, \tag{4}$$

where C_n is the neutrophil concentration on the interstitial fluid and λ_{nb} is the neutrophils phagocytosis rate [13].

The next differential model represents the neutrophil dynamics:

$$\begin{cases} \dfrac{\partial(\phi_f C_n)}{\partial t} = \nabla\cdot(D_n\phi_f\nabla C_n - \chi_{nb}\phi_f C_n\nabla C_b) - r_n + q_n & \text{in } \Omega\times I, \\ (D_n\phi_f\nabla C_n + \chi_{nb}\phi_f C_n\nabla C_b)\cdot\vec{n} = 0 & \text{in } \partial\Omega\times I, \\ C_n(\cdot,0) = C_{n0} & \text{in } \Omega, \end{cases} \tag{5}$$

where $C_n : \Omega\times I \to \mathbb{R}^+$ is the neutrophil concentration on the interstitial fluid, D_n is the diffusion coefficient of the neutrophil in the interstitial tissue, χ_{nb} is the neutrophil chemotaxis rate, q_n is the neutrophil source, which represents the neutrophil extravasation from bloodstream to interstitium, and r_n denotes the neutrophil death due to apoptosis.

The neutrophil growth function models the extravasation from capillaries to the interstitium and is represented by:

$$q_n = \gamma_n C_b(C_{n,max} - C_n), \tag{6}$$

where $\gamma_n = L_n(S/V)$, L_n is the permeability of the capillaries to neutrophils, and (S/V) is the vessel surface area per volume unit, and $C_{n,max}$ is the neutrophil concentration in the bloodstream.

The function r_n denotes the neutrophil death due to both bacterial phagocytosis and apoptosis. These events are mathematically represented by:

$$r_n = \lambda_{bn}\phi_f C_n C_b + \mu_n\phi_f C_n, \tag{7}$$

where λ_{bn} represents the death rate after phagocytosis and μ_n represents the natural neutrophil decay, once they are preprogrammed to die, in a short time, after they leave the bloodstream [4].

2.1.2. Hydro-mechanical model for inflammatory edema

In essence, the stresses related to the interstitium are composed of two parts: one which is caused by the hydrostatic pressure of the interstitial fluid filling the pores, and the other caused by the average stress in the solid part, *i.e.* the extracellular matrix and tissue cells.

Then, considering a fluid-saturated porous medium Ω that represents a living body tissue, an n-phase system of continuity equations may be used. In this system, one of the equations models the fluid and the other the solid phase. The fluid phase is mainly composed of blood plasma and the solid phase represents the extracellular matrix along with the tissue cells. The system is given by:

$$\begin{cases} \dfrac{\partial(\phi_f\rho_f)}{\partial t} + \nabla\cdot\left(\phi_f\rho_f v_f\right) = (q_c + q_l)\rho_f & \text{for the fluid phase,} \\ \dfrac{\partial(\phi_s\rho_s)}{\partial t} + \nabla\cdot(\phi_s\rho_s v_s) = 0 & \text{for the solid phase,} \end{cases} \tag{8}$$

where q_c and q_l represent the capillary bed network and the lymphatic system influence in Ω, respectively. In addition, ϕ_α, ρ_α and v_α are porosity, density and velocity for each phase, where $\alpha = f$ for fluid and $\alpha = s$ for solid.

Following our previous work [14], Eq. (9) models q_c and Eq. (12) models q_l in the fluid phase.

$$q_c(P) = c_f(P_c - P - \sigma(\pi_c - \pi_i)), \tag{9}$$

where c_f is the filtering coefficient given by $L_p(S/V)$, L_p is the hydraulic permeability of the microvascular bed wall, and (S/V) is the vessel surface area per unit volume; P and P_c are the fluid pressure in the interstitium and the capillary pressure, respectively; π_c and π_i are the capillary oncotic pressure and the interstitial oncotic pressure due to the plasma protein, respectively; and the reflection coefficient to plasma proteins is denoted by $\sigma \in [0, 1]$. Eq. (9) is known as Starling Equation [28]. It has been proposed in 1896 and is still widely used in recent work [3,18,29].

For coupling the influence of the inflammatory reaction to the fluid phase, was used the same model of our previous work [14] for the hydraulic permeability and the oncotic reflection coefficient:

$$L_p(C_b) = L_{p0}(1 + c_{bp}C_b), \tag{10}$$

where L_{p0} is the health tissue hydraulic permeability of the capillary wall, C_b is the bacteria concentration, and c_{bp} is the influence of the bacterial infection in the hydraulic permeability.

The coupling of oncotic reflection coefficient with inflammatory response is given by:

$$\sigma(C_b) = \frac{\sigma_0}{(1 + c_{br}C_b)}, \tag{11}$$

where σ_0 is the oncotic reflection coefficient in a non-inflamed tissue, C_b is the bacteria concentration, and c_{br} is the bacterial influence in the reflection coefficient.

Please cite this article as: R.F. Reis, R.W. dos Santos, B.M. Rocha et al., On the mathematical modeling of inflammatory edema formation, Computers and Mathematics with Applications (2019), https://doi.org/10.1016/j.camwa.2019.03.058.

The interstitial fluid pressure influences the plasma flux of the lymphatic capillaries [3]. The influence of the lymphatic system on the interstitial fluid dynamics is modeled by:

$$\int_V q_l(P)dV = -\left(q_0\left(1+\frac{V_{max}(P-P_0)^n}{K_m^n+(P-P_0)^n}\right)\right), \tag{12}$$

where q_0 is the normal lymph flow, P_0 is the normal interstitial fluid pressure. Moreover, V_{max} is the maximum lymph flow, K_m is the half-live, *i.e.* the value of P which the lymph flow corresponds to $\frac{V_{max}}{2}$, and n is the Hill coefficient, these parameters are normally obtained by experimental data [30].

Assuming that $v_s = \frac{\partial U}{\partial t}$, Eq. (8) can be rewritten as follows:

$$\begin{cases} \dfrac{\partial(\phi_f\rho_f)}{\partial t} + \nabla\cdot\left(\phi_f\rho_f v_f\right) = (q_c+q_l)\rho_f & \text{for the fluid phase,} \\ \dfrac{\partial(\phi_s\rho_s)}{\partial t} + \nabla\cdot\left(\phi_s\rho_s\dfrac{\partial U}{\partial t}\right) = 0 & \text{for the solid phase.} \end{cases} \tag{13}$$

Furthermore, considering that densities are constant and that $\phi_s+\phi_f = 1$, then Eq. (13) can be rewritten to obtain the following equation:

$$\begin{cases} \nabla\cdot v_D + \nabla\cdot\dfrac{\partial U}{\partial t} = q_c + q_l \\ v_D = -\dfrac{K}{\mu}\nabla P, \end{cases} \tag{14}$$

where v_D is the velocity of the fluid phase under a porous media approach, K is the porous media permeability, and μ is the fluid viscosity. It is based on Darcy's Law and is often referred to as Darcy velocity [22].

One can observe that the PDE system given by Eq. (14) has only two equations for solving three unknowns: U, v_D and P. The closure of this problem comes when momentum conservation is considered for each phase:

$$\begin{cases} \nabla\cdot(\boldsymbol{\sigma_s}) + \hat{\boldsymbol{T}}_{\boldsymbol{s}} = \mathbf{0} & \text{for the solid phase,} \\ \nabla\cdot(\boldsymbol{\sigma_f}) + \hat{\boldsymbol{T}}_{\boldsymbol{f}} = \mathbf{0} & \text{for the fluid phase,} \end{cases} \tag{15}$$

where $\boldsymbol{\sigma_f}$ and $\boldsymbol{\sigma_s}$ are the fluid and solid phases tensors, respectively, and $\hat{\boldsymbol{T}}_{\boldsymbol{f}}$ and $\hat{\boldsymbol{T}}_{\boldsymbol{s}}$ are the interaction forces between the phases.

Summing up each phase results in the following equation for the mixture:

$$\nabla\cdot(\boldsymbol{\sigma_f}+\boldsymbol{\sigma_s}) = \mathbf{0}, \tag{16}$$

where $\hat{\boldsymbol{T}}_{\boldsymbol{f}} + \hat{\boldsymbol{T}}_{\boldsymbol{s}} = 0$.

We consider the solid phase as an isotropic elastic porous medium, *i.e.* a Hookean material model [19,22]. So, the next equation is solid phase stress tensor:

$$\boldsymbol{\sigma_s} = \lambda_s(\nabla\cdot U)\boldsymbol{I} + 2\mu_s\boldsymbol{\varepsilon}(U), \tag{17}$$

where $\varepsilon(U) = \nabla U^s = \frac{1}{2}(\nabla U + \nabla U^T)$, I is the identity matrix, and λ_s and μ_s are the Lamé parameters.

The fluid phase tensor can be described according to the following relation [19,22]:

$$\boldsymbol{\sigma_f} = -P\boldsymbol{I}, \tag{18}$$

where P is the hydrostatic pressure at the interstitium and $\boldsymbol{I}$ is the identity matrix.

Finally, considering Eqs. (14) and (16) and rearranging them, can be obtained, in terms of P and U, the following system of equations:

$$\begin{cases} (\lambda_s+\mu_s)\nabla(\nabla\cdot U) + \mu_s\nabla^2 U - \nabla P = \mathbf{0}, & \text{(a)} \\ \nabla\cdot(k\nabla P) = \dfrac{3}{3\lambda_s+2\mu_s}\dfrac{\partial P}{\partial t} + q, & \text{(b)} \end{cases} \tag{19}$$

where $k = \frac{K}{\mu}$ and U is the displacements field.

2.2. Numerical methods

The finite volume method (FVM) was used to obtain an approximate solution for all PDEs given by Eqs. (2), (5), (19)(a) and (b). Let $\Omega \subset \mathbb{R}$, *i.e.* a one-dimensional domain, discretized in a set of regular nodal points defined by $S = \{(x_i)\,;\, i = 0,\ldots,I_x\}$, where I_x is the number of nodal points spaced with length Δx. Thus, Δx is the distance between right and left faces of each nodal point. Within this section we use the subscripts L and R to indicate the left and right volumes of a point P, respectively, and l and r to indicate the left and right faces of a control volume.

Eqs. (2) and (5) were solved using the FVM according to the strategy detailed in our previous work [14]. In addition, the next sections detail the discretized version of the system given by Eqs. (19)(a) and (b).

Please cite this article as: R.F. Reis, R.W. dos Santos, B.M. Rocha et al., On the mathematical modeling of inflammatory edema formation, Computers and Mathematics with Applications (2019), https://doi.org/10.1016/j.camwa.2019.03.058.

2.2.1. Hydro-mechanical model

Eq. (19)(b) was discretized using the FVM and the temporal derivatives were discretized using forward finite difference. In addition to the spatial discretization, the time domain I is partitioned into N equal time intervals of length Δt, *i.e.*, $(0, t_f] = \cup_{k=0}^{N-1}[t_k, t_{k+1}]$. Thus, Eq. (19)(b) is numerically computed by:

$$P_P^{k+1} = \frac{\Delta t}{\beta}\left(k_r \frac{P_R^k - P_P^k}{\Delta x^2} - k_l \frac{P_P^k - P_L^k}{\Delta x^2} + q^k\right) + P_P^k, \tag{20}$$

where $\beta = \frac{3}{3\lambda_s + 2\mu_s}$ and k is approximated by:

$$\begin{cases} k_l \approx \dfrac{k_P + k_L}{2k_P k_L}, \\ k_r \approx \dfrac{k_P + k_R}{2k_P k_R}. \end{cases} \tag{21}$$

Eq. (19)(a) is discretized using the FVM, resulting in Eq. (22). This linear system of equations was solved using the Jacobi method. An error smaller than 10^{-8} was adopted as the convergence criterion for the numerical solution of this equation, according to the metric $\|U_i^{k+1} - U_i^k\|_\infty$:

$$\theta_l \frac{U_R - U_P}{\Delta x} - \theta_r \frac{U_P - U_L}{\Delta x} - \frac{P_L^k - P_R^k}{2} = 0, \tag{22}$$

where $\theta = (\lambda_s + 2\mu_s)$ and is evaluated in the volume faces using the same approach presented in Eq. (21).

2.2.2. Porosity analysis

The mathematical model described by Eqs. (19)(a) and (b) was obtained summing up the equations of each phase and under the assumption that $\phi_s + \phi_f = 1$, resulting in a system of equations in which, in this case, neither ϕ_s nor ϕ_f is unknowns. However, the quantification of the fluid and the solid is important to measure the edema. So, this section describes the numerical approach used to retrieve the solid and fluid dynamics.

Let the continuity equation of the solid phase, shown in Eq. (13), be discretized using the FVM and the solid velocity discretized using the forward finite difference. So, $\frac{\partial U}{\partial t}$ is discretized as advection and, to ensure stability in the method, the First-Order Upwind (FOU) scheme was used [26].

In addition, it was also necessary to evaluate the velocities in each volume face, so the solid phase velocity, $\frac{\partial U}{\partial t}$, was discretized using a forward difference scheme.

Finally, the next equation is the discrete version of the solid phase shown in Eq. (13):

$$\phi_{s_P}^{k+1} = -\Delta t\left(\phi_{s_r}^k v_r - \phi_{s_l}^k v_l\right) + \phi_{s_P}^k \quad \text{in } \Omega, \tag{23}$$

where v_r and v_l are the velocities at right and left volume faces, respectively.

Thus, once we have the result of Eqs. (19)(a) and (b) it is possible to evaluate the solid velocity $\frac{\partial U}{\partial t}$ and solve Eq. (13) using Eq. (23).

2.3. Non-constant porosity feedback

Although Eqs. (2) and (5) were initially solved using the FVM strategy detailed in our previous work [14], in this work we also analyze the feedback of non-constant porosity at Eqs. (2) and (5) solutions.

So, considering ϕ_f non-constant in Eq. (2), we may rewrite it as follows:

$$\frac{\partial \phi_f}{\partial t} C_b + \frac{\partial C_b}{\partial t}\phi_f = \nabla \cdot (D_b \phi_f \nabla C_b) - r_b + q_b \tag{24}$$

Since, at time step n we do not have ϕ_f^{k+1} calculated yet, $\frac{\partial \phi_f}{\partial t}$ was evaluated using ϕ_f^k and ϕ_f^{k-1}. Thus, the discretized version of Eq. (2) becomes:

$$C_{b_P}^{k+1} = \frac{\Delta t}{\phi_f}\left(\Phi_b(C_b{}^k) - r_b{}^k + q_b{}^k - ({\phi_f}_P^k - {\phi_f}_P^{k-1})C_{b_P}^k\right) + C_{b_P}^k, \tag{25}$$

where

$$\Phi_b(C_b{}^k) = (D_b\phi_f)_r \frac{C_{b_E}^k - C_{b_P}^k}{\Delta x^2} - (D_b\phi_f)_l \frac{C_{b_P}^k - C_{b_W}^k}{\Delta x^2}. \tag{26}$$

An analogous assumption can be applied to Eq. (5) to obtain the following discretized version:

$$C_{n_P}^{k+1} = \frac{\Delta t}{\phi_f}\left(\Phi_n(C_n{}^k) - r_n{}^k + q_n{}^k - ({\phi_f}_P^k - {\phi_f}_P^{k-1})C_{n_P}^k\right) + C_{n_P}^k, \tag{27}$$

Please cite this article as: R.F. Reis, R.W. dos Santos, B.M. Rocha et al., On the mathematical modeling of inflammatory edema formation, Computers and Mathematics with Applications (2019), https://doi.org/10.1016/j.camwa.2019.03.058.

Table 1
Model parameters values for Eq. (2).

Name	Symbol	Unit	Value
Porosity	ϕ_f	–	0.2
Bacteria diffusion coefficient	D_b	$\frac{cm^2}{h}$	0.0001
Bacteria reproduction rate	c_b	$\frac{1}{h}$	0.15
Phagocytosis rate	λ_{nb}	$\frac{cm^3}{h.10^7 cells}$	1.8

Table 2
Model parameters values for Eq. (5).

Name	Symbol	Unit	Value
Porosity	ϕ_f	–	0.2
Neutrophil diffusion coefficient	D_n	$\frac{cm^2}{h}$	0.0001
Chemotaxis rate	χ_{nb}	$\frac{cm^5}{h.10^7 cells}$	0.0001
Induced apoptosis rate	λ_{bn}	$\frac{cm^3}{h.10^{10} cells}$	0.1
Capillary permeability to neutrophil	γ_n	$\frac{cm^3}{h.10^7 cells}$	0.1
Neutrophil source	$s_{n,max}$	–	0.55
Apoptosis rate	μ_n	$\frac{1}{h}$	0.2

where

$$\Phi_n({C_n}^k) = (D_n\phi_f)_r \frac{{C_{n_E}}^k - {C_{n_P}}^k}{\Delta x^2} - (D_n\phi_f)_l \frac{{C_{n_P}}^k - {C_{n_W}}^k}{\Delta x^2} - \left(({\chi_{nb}\phi_f {C_n}^k})_r \frac{{C_{b_E}}^k - {C_{b_P}}^k}{\Delta x} - ({\chi_{nb}\phi_f {C_n}^k})_l \frac{{C_{b_P}}^k - {C_{b_W}}^k}{\Delta x} \right). \quad (28)$$

3. Results

In this section, we present the simulation scenario and numerical results of the suggested hydro-mechanical model for inflammatory edema. To evaluate the impacts of the feedback of the mechanical deformation on the immune system, two scenarios were simulated. The first one considers that ϕ_f assumes a constant value, *i.e.* a one-way coupling is considered. The second one considers a non-constant value of ϕ_f, *i.e.* the feedback is considered.

The coupling strategy results in a complex PDE system with 4 variables and 28 parameters. For this reason, as a first approach, all the results were presented and analyzed in a one-dimensional domain. Thus, it is easier to comprehend the obtained results and discuss them. Furthermore, the entire simulation demands about 13 s when performed on an Intel Q9400 processor with 4 cores of 2.66 GHz each.

3.1. Simulation scenario

A summary of all parameter names, symbols, units and their respective values used for the immune system model in Eqs. (2) and (5) are shown in Tables 1 and 2, respectively. These values were taken from previous work [14].

In addition, a summary of all parameter names, symbols, units and their respective values used for the mechanical model in Eqs. (19)(a) and (b) are shown in Table 3.

Furthermore, the caliber of the lymphatics capillaries is greater than the blood ones, once the diameter of the lymphatic capillaries is about 0.2 mm and the blood capillaries diameter is between 5 and 10 μm [3]. The lymph vessels represent about 2.9% of a tissue [31]. So, to perform simulations the lymph vessels were randomly placed over the domain using a uniform distribution with 2.9% of probability. Otherwise, the tissue was only under blood capillary influence.

To perform the simulations, it is also necessary to set up properly the boundary and initial condition of Eqs. (2), (5), (19)(a) and (b). All their functions and values are shown in Table 4. In order to ensure a unique solution of Eq. (19)(a), it was also considered that $U = 0$ at $x = 0.5$ cm.

3.2. Simulation results

3.2.1. Edema formation

First, we analyzed the influence of immune system model to the hydro-mechanical model, so the following bacteria–neutrophil model results assume that $\phi_f = 0.2$, despite ϕ_f changes over each simulation time in the hydro-mechanical model, *i.e.* we consider one-way coupling.

Figs. 1A and C show the interactions between a bacterial infection and neutrophils, representing the immune response for an invading pathogen. These figures present the numerical solution of Eqs. (2) and (5), respectively.

Please cite this article as: R.F. Reis, R.W. dos Santos, B.M. Rocha et al., On the mathematical modeling of inflammatory edema formation, Computers and Mathematics with Applications (2019), https://doi.org/10.1016/j.camwa.2019.03.058.

Table 3
Model parameters values for Eqs. (19)(a) and (b).

Name	Symbol	Unit	Value
Interstitial pressure	P	mmHg	–
Capillary pressure	P_c	mmHg	20.0
Viscosity	μ	$\frac{g}{cm.s}$	*
Permeability	K	cm^2	*
Filtering coefficient	c_f	$\frac{1}{s.mmHg}$	–
Hydraulic conductivity	L_{p0}	$\frac{cm}{s.mmHg}$	3.6×10^{-8}
Osmotic reflection coefficient	σ_0	–	0.91
Capillary oncotic pressure	π_c	mmHg	20.0
Interstitial oncotic pressure	π_i	mmHg	10.0
Bacterial influence in hydraulic permeability	c_{bp}	$\frac{cm^3}{10^{10}cells}$	10.0
Normal lymph flow	q_0	$\frac{cm}{s}$	0.001
Lymph flow threshold	V_{max}	–	20.0
Increase flow velocity	K_m	mmHg	5.5
Initial pressure	P_0	mmHg	0.0
Exponent	n	–	7.0
Lamé's first parameter	λ_s	kPa	27.293
Shear modulus	μ_s	kPa	3.103
Displacements	U	cm	–

Table 4
Initial and boundary conditions for the model.

Variable	Initial condition	Boundary condition
C_n	$C_n = 0.0 \ \forall \ x \in \Omega$	$D_n \nabla C_n \cdot \vec{n} = 0.0 \ \forall \ x \in \partial\Omega$
C_b	$C_b = \begin{cases} 0.5 \times 10^{10} & \text{for } x = 0.5 \\ 0.0 & \text{otherwise} \end{cases}$	$D_b \nabla C_b \cdot \vec{n} = 0.0 \ \forall \ x \in \partial\Omega$
P	$P = 0.0 \ \forall \ x \in \Omega$	$\frac{K}{\mu} \nabla P \cdot \vec{n} = 0.0 \in \partial\Omega$
U	–	$\nabla U \cdot \vec{n} = 0.0 \in \partial\Omega$

The numerical solutions of Eqs. (19)(b) and (a) *i.e.* the hydro-mechanical model, are shown in Figs. 1E and G, respectively. They represent the displacements field due to the dynamics of the interstitial fluid pressure. It is important to notice that Eq. (19)(a) is not time dependent, but the results are presented along time once that, at each time, the pressure gradient changes, and it is necessary to solve Eq. (19)(a) again.

Furthermore, Fig. 1E also presents the positions where lymph vessels are seated over the domain. The triangles at the bottom of the x-axis represent the positions of lymph vessels. Thus, the pressure is smaller in the solution points under the influence of the lymphatic system than in the surrounding points, leading to a local pressure gradient.

Fig. 1I shows the numerical results of the fluid phase part of Eq. (13). Although the discretization discussed in Section 2.2.2 presents the numerical method used to solve the solid phase, Fig. 1I shows the fluid phase by using the relation $\phi_s + \phi_f = 1$. So, this figure expresses the evolution of the fluid phase over the simulated domain.

Panels on the right of Fig. 1 show the results of the same simulation presented on the left, but the time spatiotemporal dynamics are represented using space–time plots, which gives detailed evolution of the dynamics of populations along the simulation.

3.2.2. Influence of non-constant porosity

On one hand, the results shown in Figs. 1A, B, C and D represent the interactions between a bacterial infection and neutrophils, but considering a constant porosity $\phi_f = 0.2$. On the other hand, we have considered a non-constant porosity to obtain our hydro-mechanical model. Thus, it is also important to analyze the influence of the non-constant porosity on the inflammatory model, *i.e.* to consider a two-way coupling. So, for this simulation scenario, we are going to use ϕ_f changing along each simulation time for the bacteria–neutrophil model.

Once we consider the influence of non-constant porosity, Fig. 2 shows the new numerical solution of the mathematical model.

Fig. 3 shows, for comparative purposes, the bacterial and neutrophil concentration, using both constant and non-constant ϕ_f at $t = 20$ h, along with the respective values ϕ_f at the same instant of time. It is important to notice that the bacterial concentration increases along with the fluid phase when compared with the constant ϕ_f version. This is an effect of fluid accumulation on infection site, *i.e.* while the inflammatory response occurs there is an accumulation of fluid in the infection site, and, once the neutrophils come from the capillaries and its amount is constant, it decreases the concentration of neutrophil in this area.

Please cite this article as: R.F. Reis, R.W. dos Santos, B.M. Rocha et al., On the mathematical modeling of inflammatory edema formation, Computers and Mathematics with Applications (2019), https://doi.org/10.1016/j.camwa.2019.03.058.

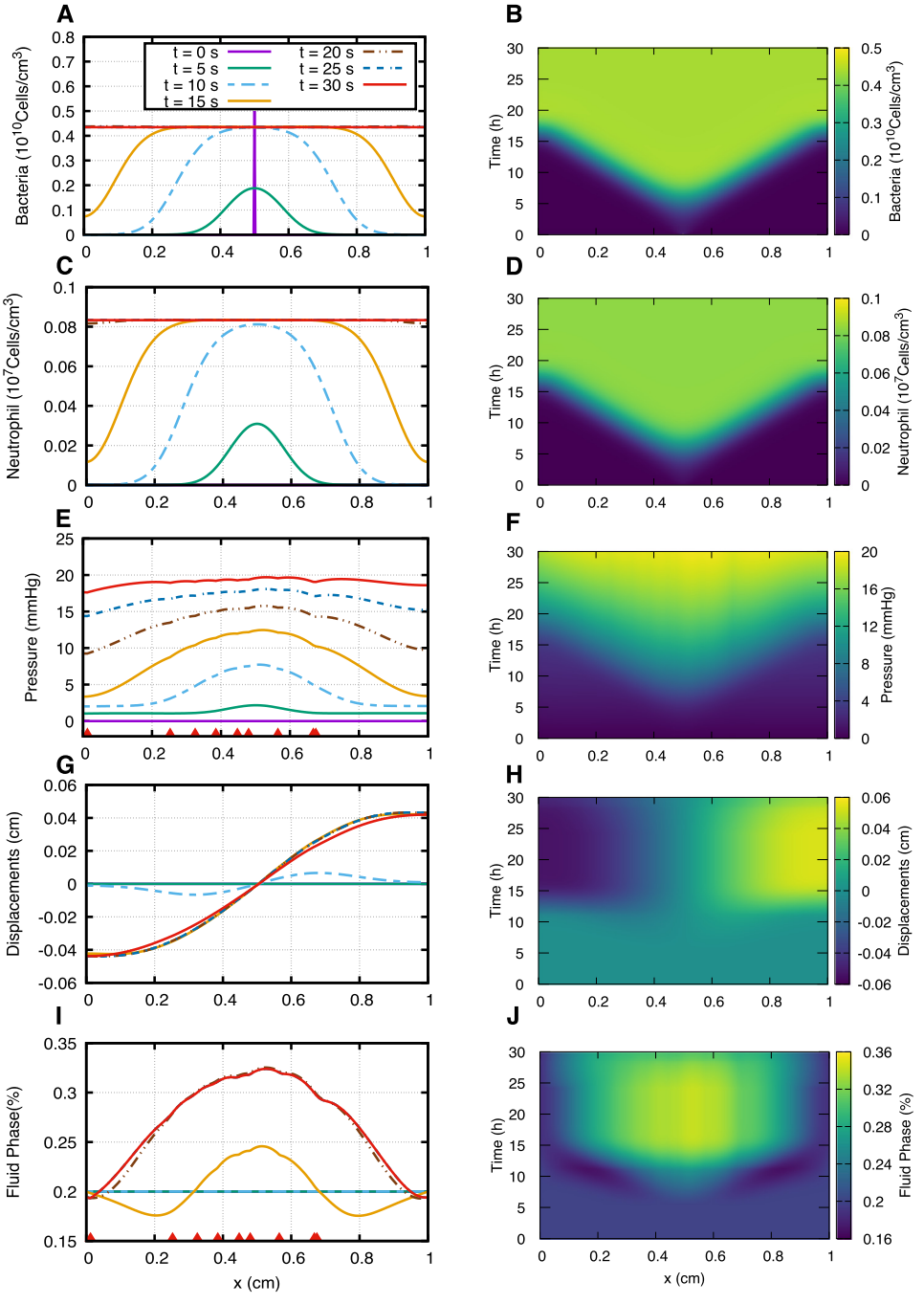

Fig. 1. Simulation results of the edema formation using Eqs. (2), (5), (19)(b), (19)(a) and (13) considering the model parameters presented in Tables 1–3 with initial and boundary conditions defined in Table 4. All panels on the right column are the same simulation of those on the left column, but the right is using space–time plot. Panels A, B, C and D show the interactions between a bacterial infection and neutrophils considering an initial infection at $x = 0.5$ cm, while panels E, F, G and H show its consequences to interstitial fluid pressure and the displacement field. Panels I and J express the evolution of the fluid phase over the simulated domain triggered by the inflammatory response. The red triangles at the bottom of panels E and I show the exact positions where lymph vessels are placed.

3.2.3. *Influence of the parameters in the model*

This section shows the influence of two model parameters in the simulation results. This analysis is performed using the one-way coupling model. It was chosen Young Modulus and lymphatic vessel amount due to their variability in different

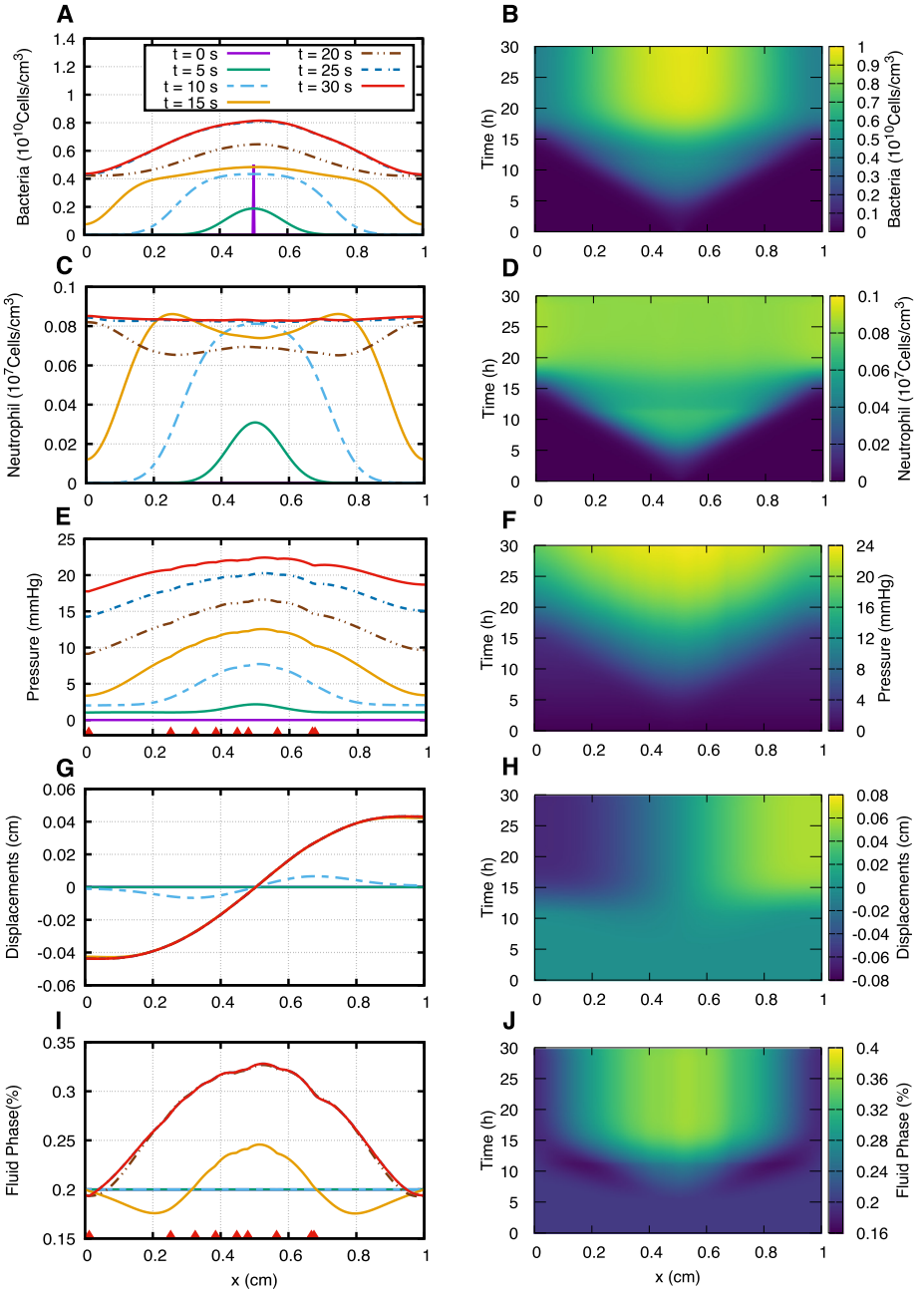

Fig. 2. Results for the simulation of the immune system with non-constant porosity feedback using Eqs. (2), (5), (19)(b), (19)(a) and (13), considering the model parameters presented in Tables 1–3, and with initial and boundary conditions defined in Table 4. To consider the non-constant porosity feedback, this simulation uses Eqs. (25) and (27) for solving Eqs. (2) and (5), respectively. All panels on the right column are the same simulations of those on the left column, but the right is using space–time plot. Panels A, B, C and D show the interactions between a bacterial infection and neutrophils, considering an initial infection at $x = 0.5$ cm, while panels E, F, G and H show its consequences to interstitial fluid pressure and the resulting displacement field. Panels I and J express the evolution of the fluid phase over the simulated domain that triggered the inflammatory response. The red triangles at the bottom of panels C and E show the exact position where the lymph vessels are placed.

living tissues and illness. For instance, the stiffness changes according to the tissue, *e.g.* bones, brain, liver, heart, and others [32–34]. In addition, some diseases may influence lymphangiogenesis [35].

Fig. 4 shows the influence of Young modulus, E, in our suggested model. It is important to notice that all results presented in Figs. 4A, B and C are the interstitial fluid pressure, displacements and fluid phase at $t = 30$ h, respectively. Since the presented mechanical model was defined as function of Lamé's first parameter, λ_s, and Shear modulus, μ_s, we

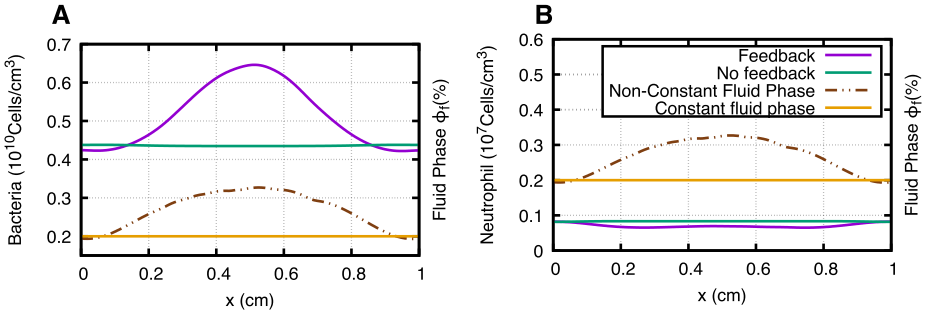

Fig. 3. Comparison between the immune system model solution considering one-way and two-way coupling at $t = 20$ h. Figs. A and B show the dynamics of immune system model (Eqs. (2) and (5), respectively) taking into account the influence of non-constant fluid phase feedback. The "Feedback" version considers the evolution of fluid phase during the simulation and the "No feedback" one considers only the constant initial value.

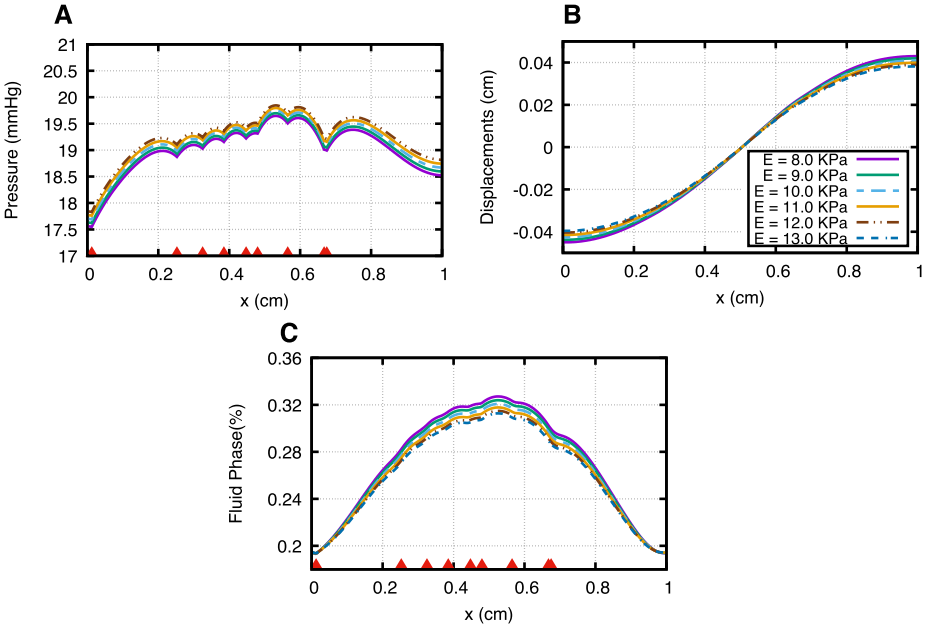

Fig. 4. Model sensitivity to Young Modulus varying according to Table 5. Panels A, B and C show the interstitial fluid pressure, displacements and fluid phase at $t = 30$ h using Eqs. (19)(b), (19)(a)and (13), respectively. The red triangles at the bottom of panels A and C show the exact position where the lymph vessels are placed.

Table 5
Mechanical properties values used in the sensibility analysis of the Young Modulus.

E (kPa)	μ_s (kPa)
8.0	2.751
9.0	3.106
10.0	3.463
11.0	3.823
12.0	4.186
13.0	4.550

have the following relation:

$$E = \frac{\mu_s(3\lambda_s + 2\mu_s)}{\lambda_s + \mu_s}. \tag{29}$$

Table 5 presents the parameters values obtained by distinct E values. Since Eq. (29) relates E with λ_s and μ_s, we vary the Young modulus and obtain a different value of μ_s by fixing the $\lambda_s = 27.293$.

Please cite this article as: R.F. Reis, R.W. dos Santos, B.M. Rocha et al., On the mathematical modeling of inflammatory edema formation, Computers and Mathematics with Applications (2019), https://doi.org/10.1016/j.camwa.2019.03.058.

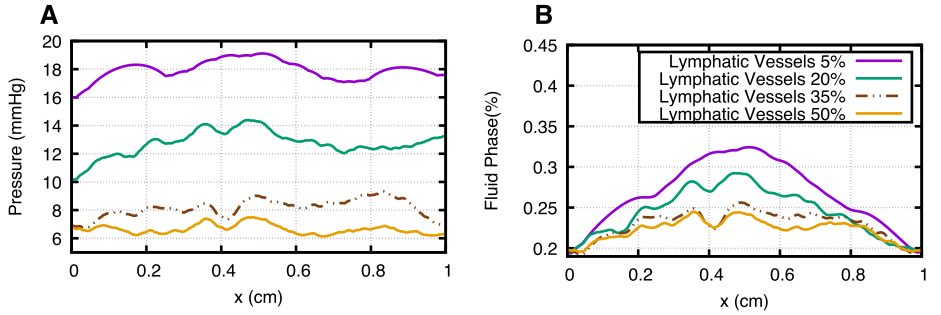

Fig. 5. Model sensitivity to lymphatic vessels growth. Panels A and B show the interstitial fluid pressure and fluid phase at $t = 30$ h using Eqs. (19)(b) and (13), respectively. Both analyses consider different amount of lymphatic vessels uniformly distributed in the simulated domain varying from 5% to 50%.

Figs. 5A and B show the influence of lymphangiogenesis in the simulated scenario. It is important to notice that all results presented in Figs. 5A and B are the interstitial fluid pressure and the fluid phase on $t = 30$ h. To perform this analysis, the lymph vessels were randomly placed over the domain using a uniform distribution varying from 5% to 50% of probability. Otherwise, the tissue was only under blood capillary influence.

4. Discussion

The first presented solution was related to the interaction between bacteria and neutrophils, *i.e.* the immune system model. It is worth to notice that the simulated scenario starts with an initial infection seated at $x = 0.5$ that spreads over time along the simulated tissue. The simulation starts with no neutrophils along the tissue and from the instant that bacteria start to proliferate, neutrophils start to enter the tissue from the bloodstream. Moreover, we force a scenario that neutrophils and bacteria coexist to analyze the mechanical deformation of the simulated tissue, but it must be stressed that this immune model is able to reproduce a scenario in which the infection vanishes [13].

On one hand, the computational model of the immune system is represented only by the neutrophils and the human immune system has many other agents besides them. On the other hand, the neutrophils represent about 70% of the white blood cells in the bloodstream, so it is a feasible approximation [4].

The second presented model was the hydro-mechanical one. Our previous work does not consider the mechanical model, and there was no fluid accumulation, once the porosity was considered constant [14]. But the edema is the result of fluid accumulation in the affected area [3,29], which in our case is caused by an inflammatory process. Thus, the edema formation is only possible by considering the mechanical deformation.

So, analyzing the results we may observe the key aspects of the edema formation process as follows: the bacterial infection spreads over the domain (see Figs. 1A and B) leading to an inflammatory reaction (see Figs. 1C and D) which changed the interstitial fluid dynamics (see Figs. 1E and F). Finally, this chain of events led to a fluid accumulation at the infected site (see Figs. 1I and J). The acute phase of an inflammatory response normally occurs between 4 and 6 h after the infection begins [1] and, in some cases, may lead to edema, which is in accordance with the results presented in Figs. 1 and 2. In addition, during inflammatory responses to infections, the literature [36,37] describes that the order of magnitude of bacterial concentration (given in bacteria/ml) is 10^9 and that the neutrophil concentration (neutrophil/ml) is 10^6. The same order of magnitude was obtained in our simulated results, as Figs. 1 and 2 show.

After showing the results of inflammatory model considering a constant porosity ϕ_f, we also present the results including the influence of the non-constant porosity, *i.e.* the feedback of fluid accumulation in our immune system model. While the fluid starts to accumulate the concentration of neutrophil decreases, as observed at $t = 20h$. It allows the bacterial colony to increase in the edematized area, but afterward neutrophil concentration goes back to its stability solution.

The last presented result was the sensitivity analysis of the model in relation to Young modulus and lymphatic vessels area. In essence, Young modulus is a mechanical property representing the stiffness of a material. In our case, it varies according to the living tissues [32–34]. Furthermore, lymphatic vessels amount also varies according to the living tissue function and diseases. For instance, lymphatic vessel area density may be around 60% of tissue in chronic airway inflammation [35].

Figs. 4B and C show the deformation and fluid accumulation into the tissue for simulations using distinct Young modulus values, and it can be observed that they were inversely proportional to this parameter, as expected. Furthermore, Fig. 4A also shows the pressure distribution using distinct values for the Young modulus, but this time results are directly proportional to this parameter, so the stiffer the tissue is, the higher is the pressure necessary to deform it. Thus, the proposed model is able to reproduce deformation in tissues with different stiffness values. Moreover, Figs. 5A and B show the influence of lymphatic vessels in the interstitial fluid pressure and in the fluid phase, respectively. These figures show

Please cite this article as: R.F. Reis, R.W. dos Santos, B.M. Rocha et al., On the mathematical modeling of inflammatory edema formation, Computers and Mathematics with Applications (2019), https://doi.org/10.1016/j.camwa.2019.03.058.

that an increase in the number of lymphatic vessels is responsible for reducing both pressure and fluid accumulation into the tissue. This is expected behavior, since the lymphatic system role is to collect the fluid and proteins filtered from the capillaries into the interstitium back to the circulatory system, working as a safety factor against edema formation [3].

5. Conclusions and future work

The present study suggested a mathematical model for inflammatory edema. Previous studies have proposed a strategy for coupling a simplified immune system model with the interstitial plasma flow equation, resulting in a model which reproduces some key aspects related to an initial edema formation, but without taking into account the fluid accumulation. Fundamentally, our previous work considers that the porosity is constant to simplify the model, so if the solid phase does not change, the fluid remains also constant. In order to allow the fluid accumulation, the current study was based on the hydro-mechanical effects in a poroelastic material. The poroelasticity theory couples Darcy's law and solid mechanics to assess deformation of porous media that results from solid consolidation. Finally, for coupling the immune system model with the poroelasticity theory were considered the same assumptions made in our previous studies, *i.e.* Eqs. (10) and (11).

The major contribution of this work is the coupling strategy of the immune system with the mechanical deformation which allows the simulation of the fluid accumulation observed in edemas. The presented model also demonstrates to be feasible in different scenarios, like different mechanical properties and lymphatic system structures. It is important to emphasize that this study takes into account all key aspects described on edema due to inflammatory response and it is able to reproduce the pathophysiology of a permeability edema formation in an inflammation.

Despite results being presented in a one-dimensional domain, they take into account key aspects of the simulated phenomenon such as: (1) the increase of permeability, which is manifested as the reduction in the osmotic reflection coefficient σ and the increase in hydraulic conductivity L_p; (2) as a consequence, capillary pressure increases in the infected site; (3) along with the higher influx of plasma fluid from bloodstream to interstitial tissue, the lymphatic system increases the lymph flow; (4) under such conditions, there is an increase in the interstitial fluid pressure and in the lymph flow, which provides a margin of safety against edema formation.

Future extensions of the present work could analyze this model using specific bacteria and/or living tissues, aiming to validate the mechanical results with experimental data. The simulations performed in a one-dimensional domain have some limitations, specially when some geometrical aspects, such as anisotropic advection–diffusion and complex domains shapes, must be taken into account. In the near future, we plan to extend the model to two and three dimensions using patient specific geometries.

Acknowledgments

The financial support by CAPES, Brazil, CNPq, Brazil, UFJF, Brazil and FAPEMIG, Brazil is greatly acknowledged.

References

[1] R.A. Goldsby, T.J. Kindt, J. Kuby, B.A. Osborne, Immunology, fifth ed., W. H. Freeman, 2002.
[2] M.J. Kluger, Body temperature changes during inflammation: their mediation and nutritional significance, Proc. Nutr. Soc. 48 (3) (1989) 337–345.
[3] A. Guyton, J. Hall, Textbook of Medical Physiology, Guyton Physiology Series, Elsevier Saunders, 2006.
[4] L. Sompayrac, How the Immune System Works, Wiley-Blackwell, 2012.
[5] A.D. Kennedy, F.R. DeLeo, Neutrophil apoptosis and the resolution of infection, Immunol. Res. 43 (1) (2009) 25–61, http://dx.doi.org/10.1007/s12026-008-8049-6.
[6] G. Laine, S. Allen, Left ventricular myocardial edema. lymph flow, interstitial fibrosis, and cardiac function, Circ. Res. 68 (6) (1991) 1713–1721.
[7] I. Eitel, M.G. Friedrich, T2-weighted cardiovascular magnetic resonance in acute cardiac disease, J. Cardiovasc. Magn. Reson. 13 (1) (2011) 13.
[8] N.C. Staub, Pulmonary edema, Physiol. Rev. 54 (3) (1974) 678–811.
[9] S.G. Rockson, Lymphedema, Am. J. Med. 110 (4) (2001) 288–295, http://dx.doi.org/10.1016/S0002-9343(00)00727-0.
[10] A.B. Pigozzo, G.C. Macedo, R.W. dos Santos, M. Lobosco, On the computational modeling of the innate immune system, BMC Bioinform. 14 (Suppl. 6) (2013) S7, http://dx.doi.org/10.1186/1471-2105-14-S6-S7.
[11] K.J. Painter, J.A. Sherratt, Modelling the movement of interacting cell populations, J. Theoret. Biol. 225 (3) (2003) 327–339, http://dx.doi.org/10.1016/S0022-5193(03)00258-3, URL http://www.sciencedirect.com/science/article/pii/S0022519303002583.
[12] E.F. Keller, L.A. Segel, Model for chemotaxis, J. Theoret. Biol. 30 (2) (1971) 225–234, http://dx.doi.org/10.1016/0022-5193(71)90050-6.
[13] A.B. Pigozzo, G.C. Macedo, R. Weber dos Santos, M. Lobosco, Computational modeling of microabscess formation, Comput. Math. Methods Med. (2012) http://dx.doi.org/10.1155/2012/736394.
[14] R.F. Reis, R.W. dos Santos, J. de Oliveira Campos, M. Lobosco, Interstitial pressure dynamics due to bacterial infection, Mecánica computacional, Bioeng. Biomech. (B) 34 (1) (2016) 1181–1194.
[15] R.F. Reis, R.W. dos Santos, M. Lobosco, A plasma flow model in the interstitial tissue due to bacterial infection, in: Lecture Notes in Computer Science, 2016, pp. 335–345, http://dx.doi.org/10.1007/978-3-319-31744-1_30.
[16] L. Cattaneo, P. Zunino, A computational model of drug delivery through microcirculation to compare different tumor treatments, Int. J. Numer. Methods Biomed. Eng. 30 (11) (2014) 1347–1371, http://dx.doi.org/10.1002/cnm.2661, URL http://dx.doi.org/10.1002/cnm.2661.
[17] R.K. Jain, J.D. Martin, T. Stylianopoulos, The role of mechanical forces in tumor growth and therapy, Annu. Rev. Biomed. Eng. 16 (2014) 321.
[18] C. Phipps, M. Kohandel, Mathematical model of the effect of interstitial fluid pressure on angiogenic behavior in solid tumors, Comput. Math. Methods Med. (2011).
[19] M.A. Biot, General theory of three-dimensional consolidation, J. Appl. Phys. 12 (2) (1941) 155–164.
[20] A.C. Rocha, M.A. Murad, C. Moyne, S.P. Oliveira, T.D. Le, A new methodology for computing ionic profiles and disjoining pressure in swelling porous media, Comput. Geosci. 20 (5) (2016) 975–996.

Please cite this article as: R.F. Reis, R.W. dos Santos, B.M. Rocha et al., On the mathematical modeling of inflammatory edema formation, Computers and Mathematics with Applications (2019), https://doi.org/10.1016/j.camwa.2019.03.058.

[21] M. Bause, F. Radu, U. Köcher, Space–time finite element approximation of the biot poroelasticity system with iterative coupling, Comput. Methods Appl. Mech. Eng.
[22] A.H.-D. Cheng, Poroelasticity, vol. 27, Springer, 2016.
[23] A. Selvadurai, A. Suvorov, Coupled hydro-mechanical effects in a poro-hyperelastic material, J. Mech. Phys. Solids 91 (2016) 311–333.
[24] A. Suvorov, A. Selvadurai, On poro-hyperelastic shear, J. Mech. Phys. Solids 96 (2016) 445–459.
[25] L. Berger, R. Bordas, K. Burrowes, V. Grau, S. Tavener, D. Kay, A poroelastic model coupled to a fluid network with applications in lung modelling, Int. J. Numer. Methods Biomed. Eng. 32 (1) (2016) http://dx.doi.org/10.1002/cnm.2731, n/a–n/a.
[26] H. Versteeg, W. Malalasekra, An Introduction To Computational Fluid Dynamics: The Finite Volume Method, second ed., Prentice Hall, 2007.
[27] B.E. McDonald, J. Ambrosiano, High-order upwind flux correction methods for hyperbolic conservation laws, J. Comput. Phys. 56 (3) (1984) 448–460.
[28] E.H. Starling, On the absorption of fluids from the connective tissue spaces, J. Physiol. 19 (4) (1896) 312–326.
[29] J. Scallan, V.H. Huxley, R.J. Korthuis, Capillary Fluid Exchange: Regulation, Functions, and Pathology, vol. 2, Morgan & Claypool Life Sciences, 2010.
[30] J.P. Keener, J. Sneyd, Mathematical Physiology, vol. 8, Springer, 1998.
[31] J.-F. Rahier, S. De Beauce, L. Dubuquoy, E. Erdual, J.-F. Colombel, A. Jouret-Mourin, K. Geboes, P. Desreumaux, Increased lymphatic vessel density and lymphangiogenesis in inflammatory bowel disease, Aliment. Pharmacol. Ther. 34 (5) (2011) 533–543.
[32] S. Budday, G. Sommer, C. Birkl, C. Langkammer, J. Haybaeck, J. Kohnert, M. Bauer, F. Paulsen, P. Steinmann, E. Kuhl, G. Holzapfel, Mechanical characterization of human brain tissue, Acta Biomater. 48 (Suppl. C) (2017) 319–340, http://dx.doi.org/10.1016/j.actbio.2016.10.036.
[33] A. Nava, E. Mazza, M. Furrer, P. Villiger, W. Reinhart, In vivo mechanical characterization of human liver, Med. Image Anal. 12 (2) (2008) 203–216, http://dx.doi.org/10.1016/j.media.2007.10.001.
[34] Y.-C. Fung, Biomechanics: Mechanical Properties of Living Tissues, second ed., Springer-Verlag New York, 1993.
[35] P. Baluk, T. Tammela, E. Ator, N. Lyubynska, M.G. Achen, D.J. Hicklin, M. Jeltsch, T.V. Petrova, B. Pytowski, S.A. Stacker, S. Ylä-Herttuala, D.G. Jackson, K. Alitalo, D.M. McDonald, Pathogenesis of persistent lymphatic vessel hyperplasia in chronic airway inflammation, J. Clin. Investig. 115 (2) (2005) 247.
[36] A. Swidsinski, J. Weber, V. Loening-Baucke, L.P. Hale, H. Lochs, Spatial organization and composition of the mucosal flora in patients with inflammatory bowel disease, J. Clin. Microbiol. 43 (7) (2005) 3380–3389.
[37] M.S. Muhlebach, P.W. Stewart, M.W. Leigh, T.L. Noah, Quantitation of inflammatory responses to bacteria in young cystic fibrosis and control patients, Am. J. Respir. Crit. Care Med. 160 (1) (1999) 186–191.

Please cite this article as: R.F. Reis, R.W. dos Santos, B.M. Rocha et al., On the mathematical modeling of inflammatory edema formation, Computers and Mathematics with Applications (2019), https://doi.org/10.1016/j.camwa.2019.03.058.